13th International Symposium on Particle Image Velocimetry – ISPIV 2019
Munich, Germany, July 22-24, 2019

Experimental characterization of a fast heating system for microfluidic direct methanol fuel cells

Julian Massing[1*], Nadine van der Schoot[2], Christian J. Kähler[1], Christian Cierpka[3]

[1] Institute of Fluid Mechanics and Aerodynamics, Universität der Bundeswehr München, D-85577 Neubiberg, Germany

[2] The hydrogen and fuel cell center - ZBT GmbH, Carl-Benz-Str. 201, D-47057 Duisburg, Germany

[3] Institute of Thermodynamics and Fluid Mechanics, Technische Universität Ilmenau, 98684 Ilmenau,

[*] julian.massing@unibw.de

Abstract

In this work, a simple and effective heating system for microfluidic direct methanol fuel cells is investigated experimentally. The system provides a possible solution for the problem of long fuel cell start-up times due to a slow temperature rise during the initial cell operation. A thin semi-conductive heating layer is applied to the anode and cathode side cover plates and subjected to a short boost of high electrical power. The volumetric temperature and velocity fields on the anode side are measured by means of luminescence lifetime imaging and astigmatism particle tracking velocimetry. The cell's working temperature of 80 °C is reached within 25 s, thus reducing the start-up time of the fuel cell tremendously from 15 min to only 20 s.

1 Introduction

Due to the increased functionality and higher data traffic of modern portable and mobile electronic devices, the energy demand of these systems has increased significantly in recent years. In contrast, the development of the energy capacity of batteries, which are typically used as power sources in portable equipment, could not keep pace over the same period of time, leading to the well known short battery life times of smart phones, tablets, etc. Schaevitz (2012). Since methanol has a very high gravimetric energy density of 6.09 kWh/kg Munjewar et al. (2017) and is easy to store and transport, it is an ideal fuel for portable applications Kamarudin et al. (2009). Thus, microfluidic direct methanol fuel cells (μ-DMFCs), which convert the chemical energy of methanol to electrical energy (and heat), are a promising alternative power source to enable continuous and long time operation of mobile devices.

The performance of DMFCs significantly depends on the operating temperature, since the activity of the reaction layer increases with higher temperatures Scott et al. (1999). However, the details of the heat transfer in the flow field of DMFCs are not fully understood, yet Faghri and Guo (2005). During cell operation, heat is released by the methanol oxidation reaction and removed by the relatively cold anode side methanol/water flow and cathode side air flow, as well as via heat conduction and natural convection. Furthermore, cell temperature is significantly influenced by the formation of CO_2 gas bubbles on the anode side and water droplets on the cathode side. It is well known, that two-phase flow has a significant impact on heat transfer. However, the specifics are still under investigation Kandlikar et al. (2013); Wang and Wang (2006); Kandlikar and Lu (2009).

The temperature dependency plays a large role, especially during the start-up of the cell from ambient temperature, since the temperature rise during the initial cell operation is relatively slow. This leads to a similarly slow increase in output power, which causes a long start-up phase of currently available DMFC systems in the order of 15 min SFC Energy AG (2016). For portable applications, this time needs to be significantly reduced. One approach to accomplish this task is to power a DMFC with pure hydrogen during the start-up phase and then switch to methanol, thus making use of the higher heat release of the hydrogen reaction Kwon et al. (2011). However, this design significantly increases the complexity of the fuel cell system and a simpler solution is desired.

In this work, a heating system is introduced and characterized experimentally, that enables the start-up of direct methanol fuel cells within seconds, while minimizing the increase in system complexity. A thin indium tin oxide (ITO) heating layer is applied to the anode and cathode cover plates. The layer is subjected to high electrical power, which leads to a fast heating of the fuel cell. The three-dimensional temperature and velocity fields are measured experimentally by means of astigmatism particle tracking velocimetry (APTV) and luminescence lifetime imaging Massing et al. (2018), verifying the effectiveness of the heating system. The goal is to significantly reduce the starting time of the fuel cell, i.e. the time until approx. 90 % of the maximum output power of the cell is reached.

2 Fuel cell design

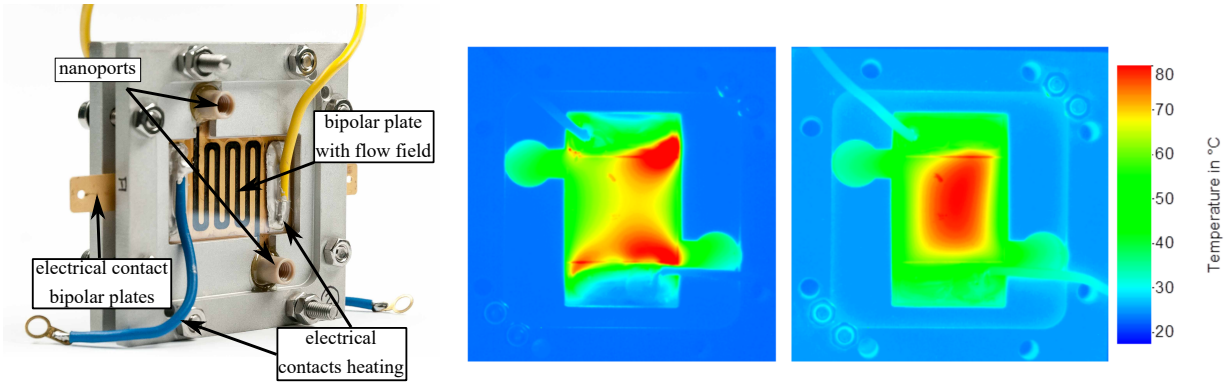

(a) (b)

Figure 1: a) Photograph of the assembeled DMFC. In the photograph, only the anode side is shown, since the cathode side has a similar design. b) Thermal image of the ITO layer during heating with an input power of 32 W. No fluid flow was applied. Left after 8.4 s, right after 5 min.

For the experiments a experimentally accessible DMFC assembly with optically accessible anode and cathode flow fields was designed and manufactured by the hydrogen and fuel cell center (ZBT GmbH) Duisburg. A photograph of the fuel cell is shown in figure 1a. The anode and the cathode bipolar half plates contain a serpentine flow field with seven channels with a nominal channel cross section of 1.7×0.55 mm^2 (width $\times$ height), a spacing of 1.5 mm and a length of 40 mm. They are made of stainless steel and coated with a 5.3 μm gold layer. The proton exchange membrane consists of Nafion 115 with a 2 mg/cm^2 platinum-ruthenium catalyst layer on the anode side and a 2 mg/cm^2 platinum catalyst layer on the cathode side. The anode gas diffusion layer is manufactured out of Sigracet 29AA and the cathode GDL is produced from Sigracet 29BC. The active area is 22.5×22.5 mm^2. The cover plates of the anode and cathode side are made out of HQ-floatglass, which is transparent for the optical measurements. To seal the DMFC, dispensed gaskets are directly applied on the bipolar plates and the assembly is compressed between two aluminum end plates. With this configuration, air tight sealing and long-time stability of the fuel cell can be ensured.

The rapid heating of the fuel cell during its start-up was realized via a thin indium tin oxide (ITO) layer applied to the glass cover plates, that served as a semi-conductive heating layer. The sheet resistance of the layer is $< 50\ \Omega$ with a thickness of 40 nm. The ITO layer is connected to a power source with a base output power of 8 W and a boost power of 32 W, which can be switched on manually. The base power is necessary to maintain a constant cell temperature of approx. 80 °C during cell operation and the boost is applied for rapid heating. The heated area is approx. 41×24 mm^2. With this system the temperature in the region of the active area is increased significantly up to 80 °C within only 8 s after the heating is turned on (see figure 1b, left). It can clearly be seen, that the temperature profile is still inhomogeneous with high temperatures close to the electrical contacts. After 5 min the temperature has become homogeneous over the entire region of the active area (see figure 1b, right). However, the question of how fast the heat is transferred to the membrane and how the temperature in the flow field and particularly near the MEA develops in time is still open. This will be investigated in the following experiments by optical methods.

3 Experimental set-up

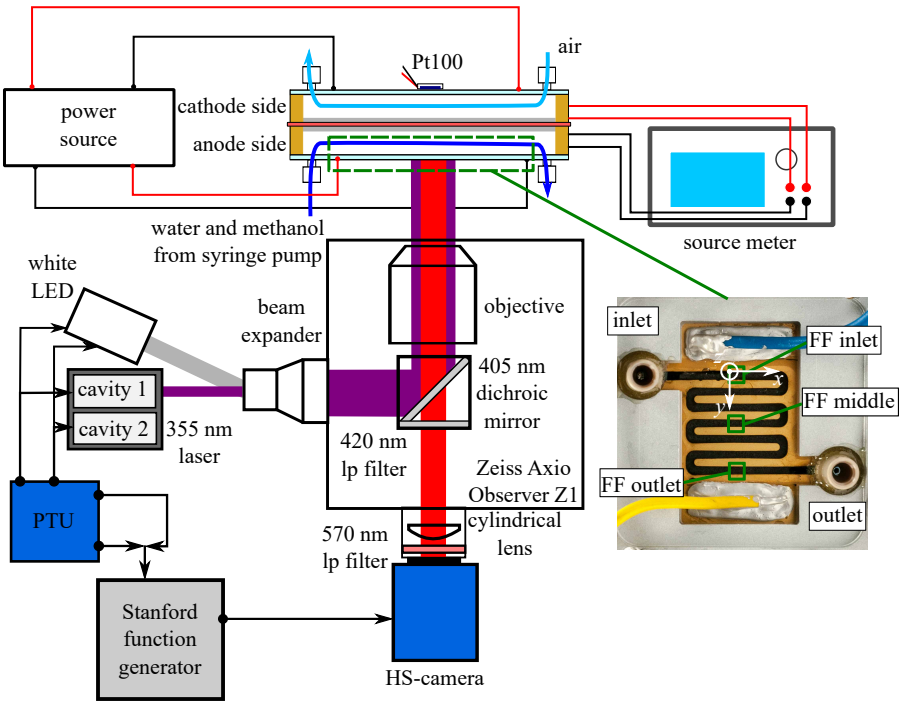

Figure 2: Schematic representation of the experimental set-up. The inset photograph shows a top view of the anode flow field illustrating the three measurement positions at the inlet, the middle and the outlet of the flow field. As indicated, the origin of the coordinate system was set at the beginning of each measurement volume, with the x-axis in main flow directions, the y-axis in spanwise direction starting at the channel wall and the z-axis in depth direction starting at the glass cover.

The experimental set-up is schematically depicted in figure 2. Galvanostatic measurements of the cell performance were carried out with a Keithley 2460 source meter. The temperature of the cover glass on the cathode side was monitored during the experiments with a Pt100 resistance thermometer that was positioned on top of the glass in the middle of the flow field. A 1 mol/l methanol and water solution was driven through the anode channel with a Cetoni neMESYS syringe pump with a constant volume flow rate of 20 ml/h which corresponds to a mass flow rate of approx. 20 g/h and a Reynolds number of Re = 4 based on the hydraulic diameter (d_h = 0.8 mm). The volumetric air flow rate on the cathode side was set constant to 100 ml/min corresponding to a Reynolds number of Re = 106.

Simultaneous measurements of the volumetric temperature and velocity fields were performed by means of luminescence lifetime imaging and APTV. The measurement technique is based on the imaging of luminescent polymer particles suspended in the flow. The velocity field can be obtained from the flow induced shift of individual particle images in time, whereas the temperature is determined simultaneously by evaluating the emission decay of individual particles Massing et al. (2018). To acquire the depth information, a cylindrical lens is introduced between the camera and the imaging optics, which breaks the axis symmetry of the optical system Cierpka et al. (2010). Thus, the previously circular particle images of spherical particles become elliptically shaped. The length of the ellipses' major axes is unambiguously related to the particles' distance from the objective lens. Therefore, the x-y-z position of the particles in space can be determined via the X-Y position of the centroid in the camera image plane as in 2D PTV Raffel et al. (2018) and the relation between the elliptical shape of the particle images and their z-position, which is determined via a proper calibration Cierpka et al. (2011). With this information, the 3D3C velocity field can be resolved by particle image tracking Cierpka et al. (2013). As tracers, polymethylmethacrylat (PMMA) particles doped with the luminescent dye europiumtristhenoyltrifluoroacetonate (EuTTa) with a mean particle diameter of 10 μm were used (Surflay Nanotec, Massing et al. (2016)). Similar to the rapid lifetime determination method two images are recorded during the temperature sensitive luminescent lifetime of EuTTa, using a

high speed camera (see figure 3a) Woods et al. (1984); Someya et al. (2013). With a proper calibration, the temperature can be determined from the ratio of the signal intensities of individual particles in the two images, i.e. I_2/I_1 and respectively I_4/I_3 in figure 3a Massing et al. (2018). As the luminescence lifetime is an intrinsic property of the luminescent molecule, it is not affected by intensity artifacts such as variations in the illumination intensity in space and time and no additional reference signal is needed Sakakibara and Adrian (2004); Kim and Yoda (2014).

The anode flow field was observed with a Zeiss Axio Observer Z1 microscope that was equipped with a 405 nm dichroic mirror which guided the illumination light to the flow field. Using a Zeiss EC Plan-Neofluar 5×/0.16 objective lens gave a field of view of approx. 2.3×1.8 mm^2. Images were recorded with a PCO Dimax HS4 high speed camera and the particles' luminescence was excited by a 355 nm Innolas Spitlight 400 Nd:YAG laser with a pulse width of 5 ns and a pulse energy of 12 mJ. A 570 nm long pass filter was placed in front of the camera to filter laser reflections. A cylindrical lens with a focal length of 1000 mm was used to induce astigmatic aberrations, which resulted in a measurement volume depth of $\Delta z \approx 350$ μm. The uncertainty of the estimation of the depth position was $\pm 2\sigma \approx \pm 15$ μm or ± 4 % of the measurement volume depth for a single particle image, which was determined from the calibration data. However, by using ensemble averaging the measurement uncertainty can be significantly reduced with the number of samples. Additionally to the temperature and velocity field, CO_2 bubbles were visualized via white LED illumination. The LED light was guided into the microscope via the beam expander that was also used for the laser illumination. The bubble images were used to automatically remove reflections of the luminescent light on the bubble interface which were erroneously detected to be particle images and may falsify the measurement results.

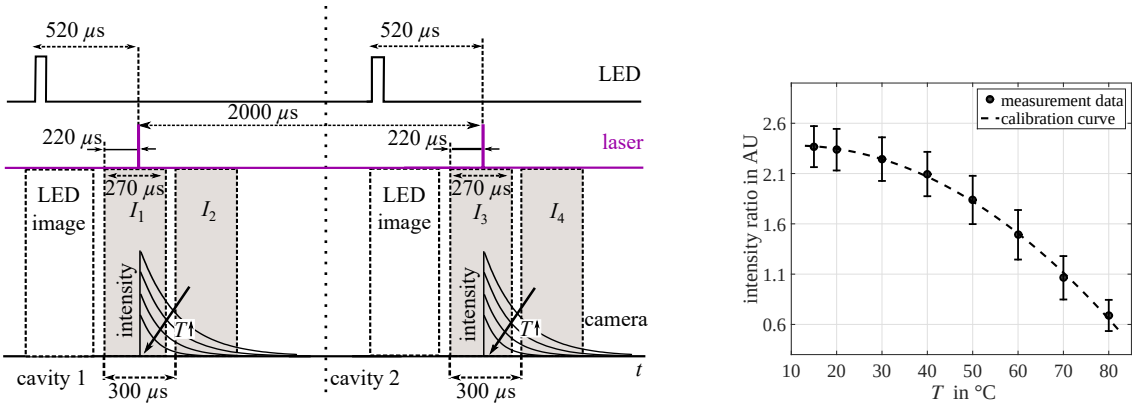

Figure 3: a) Timing sequence for temperature and velocity measurements and b) Calibration curve for temperature measurements ($< I_2/I_1 >$ over T). The error-bars show twice the standard deviation for individual particle images, which is $2\sigma \approx 8$ °C or 12 % of the measurement range.

The timing sequence utilized to record the camera images and trigger the two light sources is shown in figure 3a. To determine the velocity field with APTV, both cavities of the laser were triggered with a pulse difference of 2000 μs and the particle image displacement between the two laser pulses was related to the velocity. For each laser pulse, three images were recorded with a frame rate of approx. 3333 fps ($\Delta t = 300$ μs) and an exposure time of $\tau_{exp} = 270$ μs. The first image was triggered together with the LED light source before the laser pulse to visualize the CO_2 bubbles. Since the bubble velocity is small compared to the fluid velocity a constant bubble position within the two consecutive images can be assumed. The average temperature sensitivity of the intensity ratio between the lifetime images was approx. -1 %/K over the entire temperature range from 15 °C to 80 °C (see figure 3b). With this set-up a mean temperature uncertainty of $\pm 2\sigma \approx \pm 8$ °C or ± 12 % of the temperature range for individual particle images was achieved, which could be significantly reduced by ensemble averaging over finite volumes as done in the following.

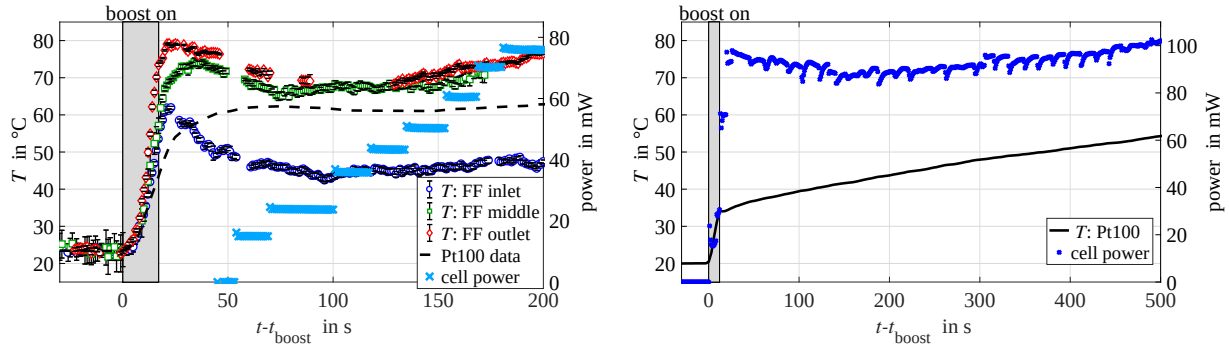

(a) (b)

Figure 4: a) Temporal evolution of the temperature close to the MEA and of the cell power at all three measurement positions. The error-bars show the 95.5 % confidence interval. Missing data points are due to gas slugs, that covered the entire observed channel section over several seconds until they were removed by the flow of the water/methanol mixture. b) Start-up of the fuel cell within 20 s.

4 Results

Measurements of the temperature and velocity field in the anode channel were performed at the inlet, the middle and the outlet of the flow field as indicated in figure 2. The very fast heating of the fuel cell after the boost is switched on at $t - t_{\text{boost}} = 0$ s can clearly be seen in figure 4a. Within only approx. 25 s a temperature of 60 °C is reached at the flow field inlet, a temperature of 70 °C is reached at the middle of the flow field and a temperature of 80 °C is reached at the flow field outlet, respectively. Since the boost is turned off at that time, the heating power reduces from 32 W to 8 W and the cell temperature is reduced due to convective cooling. Between $t - t_{\text{boost}} \approx 90$ s and 130 s the cell temperature stays relatively constant at 45 °C at the inlet and at 68 °C at the middle of the flow field. At the outlet there are only data points at the beginning and the end of this time period, due to a slug blocking that part of the channel. They give a temperature of approx. 69 °C. After $t - t_{\text{boost}} \approx 130$ s the temperature starts increasing again slowly at all three measurement positions.

Furthermore, figure 4a shows that only 180 s after heating of the cell was initialized, a cell power of 76 mW is reached, which is already 76 % of the maximum power of 100 mW. Moreover, the start-up of the cell was done conservatively, to avoid damaging the cell since the temperature in the cell was not known *a priori*. As the experiments show, the temperature in the flow field is already relatively stable at a high value shortly after heat up. Thus, the increase in cell power could be done quicker and in larger steps. Based on this conclusion, the rapid start-up capabilities of the cell were demonstrated in a subsequent experiment, in which the cell power was quickly increased right after the heating system was switched on. The development of the cell power over time is depicted in figure 4b. It can clearly be seen that 92 % of the maximum cell power is generated after only 20 s. Therefore, it can be concluded that the heating system developed within this work enables a fast start of microfluidic direct methanol fuel cells within seconds.

The cross sectional temperature field at the inlet of the flow field is depicted in figure 5a. Shortly after the boost is switched on, the temperature in the fluid increases and quickly reaches approx. 60 °C in the channel center ($t - t_{\text{boost}} = 15$ s). However, the heat flux over the channel wall is quite inhomogeneous. A spatial temperature gradient from the lower left part of the channel with higher temperatures to the upper right part of the channel with lower temperatures can clearly be seen during heating. This agrees with the infrared thermography data of the ITO-heating layer. Shortly after the boost is applied, the temperature distribution of the glass plate is quite inhomogeneous (see figure 1b). Close to the electrical contacts of the heating layer, the temperature is highest and decreases toward the middle of the flow field. Here, the electrical contact is on the left side of the inlet channel, which matches the inhomogeneous temperature distribution. Therefore, this effect is specific for the particular cells and can be altered in a later design. After the boost is turned off, the temperature in the channel decreases due to convective cooling ($t - t_{\text{boost}} = 90$ s).

In figure 5b the temperature field in the cross section at the middle of the flow field is shown. When the boost is turned on the temperature rapidly increases from ambient temperature to approx. 70 °C in the center of the cross section ($t - t_{\text{boost}} = 15$ s). In this case the heat flux is homogeneous over the glass cover plate, in agreement to the infrared measurements. It is also evident, that the temperature increase in the fluid

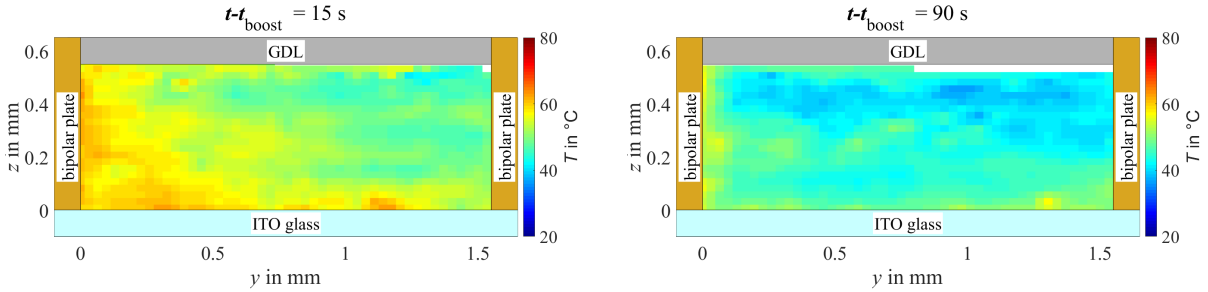

(a) Temperature distribution at the flow field inlet.

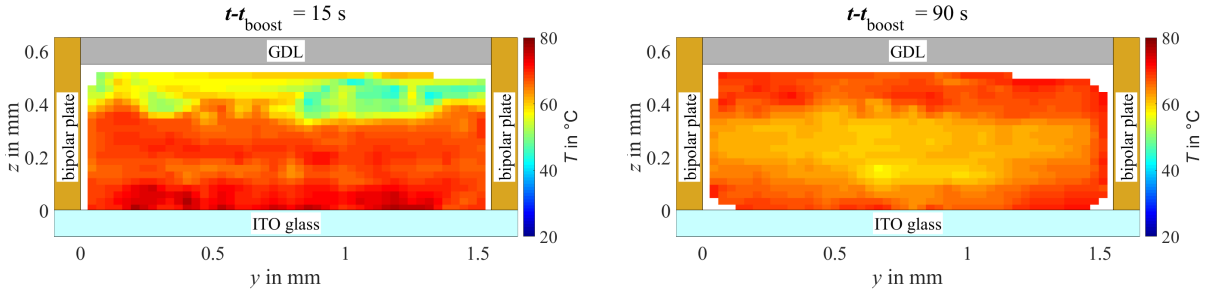

(b) Temperature distribution at flow field middle.

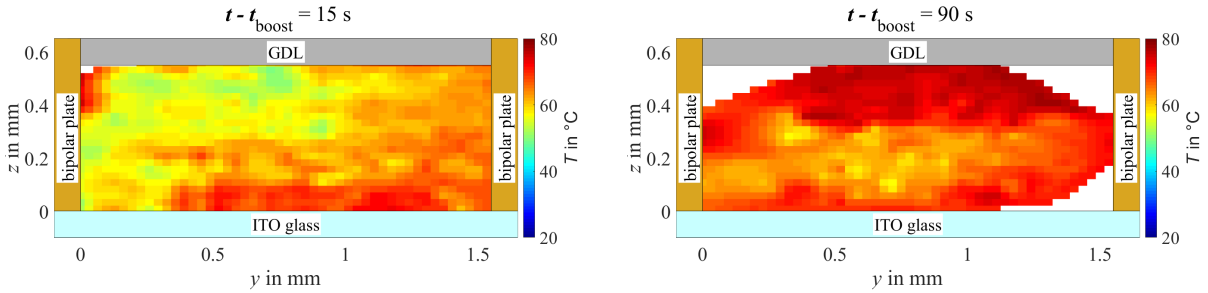

(c) Temperature distribution at flow field outlet.

Figure 5: Development of the temperature field in the cross section of the channel 15 s and 90 s after the boost is switched on, (a) at the inlet of the flow field, (b) at the middle of the flow field and (c) at the outlet of the flow field. The temperature distribution was determined by averaging the data in bins of $65 \times 33\ \mu m^2$ ($y \times z$), which corresponds to a spatial resolution of approx. 4% of the measurement volume in y-direction and 6% of the measurement volume in z-direction. Furthermore, the displayed temperature field is an ensemble average over a measurement time of 6 s and the entire field of view in x-direction.

is mainly directed from the bottom of the channel to the top. Thus, heat transfer through the cathode and anode bipolar plates toward the MEA is associated with a significant time delay. The convective cooling of the channel after the boost is turned off until $t - t_{boost} = 90$ s is again evident in the temperature field. It can also clearly be seen, that the temperature at all four channel walls is similar at this point in time. Thus, it is concluded that the temperature in the solid part of the fuel cell has reached spatial equilibrium.

Figure 5c displays the cross sectional temperature field at the outlet of the flow field. Similar to the flow field inlet a fast inhomogeneous heating of the fluid is observed within the first 15 seconds after the boost is switched on. In this channel section the spatial temperature gradient extends from higher temperatures at the bottom right of the cross section to smaller temperatures at the top left channel wall. This direction correlates with the position of the electrical contact at the anode outlet (see figure 2). As with the other measurement positions, the cooling of the channel after the boost is switched off is apparent in figure 5c.

5 Conclusion

In order to solve the problem of long start-up times of microfluidic direct methanol fuel cells associated with a slow temperature rise during start-up, a novel fuel cell design containing an electric heating layer was introduced in this work. Rapid heating of the cell was realized via a thin ITO layer that was applied to the glass cover plates of the anode and cathode sides and supplied with an electrical power of 32 W. Simultaneous volumetric measurements of temperature and velocity fields within the anode flow field were performed using luminescence lifetime imaging and APTV. The results show a fast increase of the temperature in the vicinity of the membrane, reaching a temperature of approx. 70 °C within 25 seconds after the heating power is turned on. With this heating system, a cell start-up time of 20 s was achieved.

In conclusion, the newly developed heating system introduced in this work gives a simple and effective method to significantly reduce the starting time of microfluidic direct methanol fuel cells. Thus, this work makes an important contribution to the ongoing commercialization of μ-DMFCs for portable electronic devices as a possible solution for the problem of low battery lifetimes and long charging times. Furthermore, the spatially highly resolved and accurate volumetric temperature and velocity measurement technique applied in this work enables experimental validation of CFD models for complex flow structures as in real fuel cell stacks Schmieder et al. (2016). A better understanding of the associated effects will improve current heat transfer models and provide new possibilities of efficient fuel cell design.

Acknowledgements

Financial support from the AiF under the project No. 18941 N (JM and NvS) and from the DFG through the Emmy-Noether Research group program under grant No. CI 185/3 (CC) is gratefully acknowledged.

References

Cierpka C, Lütke B, and Kähler CJ (2013) Higher order multi-frame particle tracking velocimetry. *Experiments in Fluids* 54:1–12

Cierpka C, Rossi M, Segura R, and Kähler CJ (2011) On the calibration of astigmatism particle tracking velocimetry for microflows. *Measurement Science and Technology* 22:015401

Cierpka C, Segura R, Hain R, and Kähler CJ (2010) A simple single camera 3C3D velocity measurement technique without errors due to depth of correlation and spatial averaging for microfluidics. *Measurement Science and Technology* 21:045401

Faghri A and Guo Z (2005) Challenges and opportunities of thermal management issues related to fuel cell technology and modeling. *International Journal of Heat and Mass Transfer* 48:3891–3920

Kamarudin SK, Achmad F, and Daud WRW (2009) Overview on the application of direct methanol fuel cell (DMFC) for portable electronic devices. *International Journal of Hydrogen Energy* 34:6902–6916

Kandlikar SG, Colin S, Peles Y, Garimella S, Pease RF, Brandner JJ, and Tuckerman DB (2013) Heat transfer in microchannels—2012 status and research needs. *Journal of Heat Transfer* 135:091001

Kandlikar SG and Lu Z (2009) Thermal management issues in a PEMFC stack–A brief review of current status. *Applied Thermal Engineering* 29:1276–1280

Kim M and Yoda M (2014) The spatial resolution of dual-tracer fluorescence thermometry in volumetrically illuminated channels. *Experiments in Fluids* 55:1–12

Kwon JM, Kim YJ, and Cho HJ (2011) High-efficiency active DMFC system for portable applications. *IEEE Transactions on Power Electronics* 26:2201–2209

Massing J, Kaden D, Kähler CJ, and Cierpka C (2016) Luminescent two-color tracer particles for simultaneous velocity and temperature measurements in microfluidics. *Measurement Science and Technology* 27:015301

Massing J, Kähler CJ, and Cierpka C (2018) A volumetric temperature and velocity measurement technique for microfluidics based on luminescence lifetime imaging. *Experiments in Fluids* 59:163

Munjewar SS, Thombre SB, and Mallick RK (2017) Approaches to overcome the barrier issues of passive direct methanol fuel cell–review. *Renewable and Sustainable Energy Reviews* 67:1087–1104

Raffel M, Willert CE, Scarano F, Kähler CJ, Wereley ST, and Kompenhans J (2018) *Particle image velocimetry: a practical guide*. Springer

Sakakibara J and Adrian RJ (2004) Measurement of temperature field of a Rayleigh-Bernard convection using two-color laser-induced fluorescence. *Experiments in Fluids* 37:331–340

Schaevitz SB (2012) Powering the wireless world with mems. in *Micromachining and Microfabrication Process Technology XVII*. International Society for Optics and Photonics

Schmieder F, Kinaci ME, Wartmann J, König J, Büttner L, Czarske J, Burgmann S, and Heinzel A (2016) Investigation of the flow field inside the manifold of a real operated fuel cell stack using optical measurements and computational fluid mechanics. *Journal of Power Sources* 304:155–163

Scott K, Taama WM, Kramer S, Argyropoulos P, and Sundmacher K (1999) Limiting current behaviour of the direct methanol fuel cell. *Electrochimica Acta* 45:945–957

SFC Energy AG (2016) *EFOY COMFORT User Manual V5.0*. Brunnthal

Someya S, Okura Y, Munakata T, and Okamoto K (2013) Instantaneous 2D imaging of temperature in an engine cylinder with flame combustion. *International Journal of Heat and Mass Transfer* 62:382–390

Wang Y and Wang CY (2006) A nonisothermal, two-phase model for polymer electrolyte fuel cells. *Journal of the Electrochemical Society* 153:A1193–A1200

Woods R, Scypinski S, and Love LC (1984) Transient digitizer for the determination of microsecond luminescence lifetimes. *Analytical Chemistry* 56:1395–1400